Color Mechanism and Spectroscopic Thermal Variation of Pink Spinel Reportedly from Kuh-i-Lal, Tajikistan

Yicen Liu, Lijian Qi, Dietmar Schwarz, and Zhengyu Zhou

The color mechanism of pink spinel from Kuh-i-Lal in the Pamir Mountains of Tajikistan was studied using photoluminescence, mid-infrared, and ultraviolet/visible spectroscopy. This included studying the variations in spectra after heating to a series of temperatures ranging from 300° to 1000°C. Laser ablation–inductively coupled plasma–mass spectrometry was used to measure the trace elements present. The results reveal that the color is caused by the combined effect of spin-allowed transitions of Cr^{3+}, Fe^{3+}, V^{3+}, and Fe^{2+}-Fe^{3+} intervalence charge transfer mechanisms. The photoluminescence spectra show that during heat treatment, the intensity of the N_1 peak (687 nm) and the full width half maximum of the R-line and N-lines increase with temperature. Following heating in the range of 750°–825°C, there is a linear relationship between temperature and the ratio of integral areas of the R-line and N-lines. The mid-infrared spectra indicate that the band at 581 cm^{-1} (ν_3) gradually disappears during the heating process, which is likely related to the variation of octahedral M-O and tetrahedral T-O bond length in the spinel lattice.

Spinel is a series of metal oxides with the general formula $(A_{1-i}B_i)^{IV}(A_iB_{2-i})^{VI}O_4$, in which A represents divalent cations such as Mg^{2+}, Fe^{2+}, Zn^{2+}, Mn^{2+}, Co^{2+}, or Ni^{2+}, while B represents trivalent cations such as Al^{3+}, Cr^{3+}, V^{3+}, or Fe^{3+}, IV and VI represent the tetrahedral site and octahedral site respectively, and *i* is the degree of distortion. Gem-quality spinel is composed mainly of $MgAl_2O_4$. Due to the different chromophoric ions contained within the lattice, spinel comes in a diverse range of colors. For example, spinel containing Co^{2+} is commonly blue (Shigley and Stockton, 1984; Fregola et al., 2014; Chauviré et al., 2015; Long et al., 2018). Iron-rich spinel appears blue, green, or pink when iron is the dominant minor element. When iron largely replaces magnesium in the main lattice, spinel appears black (De Souza et al., 2001; Taran et al., 2005; Lenaz and Lughi, 2013; Andreozzi et al., 2019). Cr^{3+}- and V^{3+}-bearing spinel is typically orange, red, or magenta (Malsy and Klemm, 2010; Widmer et al., 2015; Giuliani et al., 2017; Malíčková et al., 2021). Yellowish green spinel is related to high manganese content (Andreozzi et al., 2019), while high zinc content is commonly associated with a dark blue or dark green color (Fregola et al., 2014).

Spinel from the Kuh-i-Lal deposit in Tajikistan (figure 1) is mainly pink and purple, and it formed in the Goran metamorphic series of southwest Pamir Plateau. The lithology of the Golan area is high-grade metamorphic rock, and spinel occurs in the forsterite lens of magnesian skarn. These forsterite lenses generally range in length from 10 cm to 5 m, with a maximum of 30 m (Hubbard et al., 1999). At Kuh-i-Lal, spinel often coexists with enstatite, magnesite, phlo-

In Brief

- Spin-allowed transitions of Cr^{3+}, Fe^{3+}, V^{3+} , and Fe^{2+}-Fe^{3+} intervalence charge transfer lead to the color of pink spinel.
- The intensity of the R-line and N-lines at 680–692 nm in the PL spectrum are independent of the Cr^{3+} content.
- Thermal treatment widens the FWHM of R-line and N-lines, corresponding to changes in the classes of Cr^{3+} ions in spinel.
- The disappearance of the ν_3 band at 581 cm^{-1} with heating is likely related to the increasing M-O and decreasing T-O bond lengths.

See end of article for About the Authors and Acknowledgments.
Gems & Gemology, Vol. 58, No. 3, pp. 338–353,
http://dx.doi.org/10.5741/GEMS.58.3.338

gopite, pyrrhotite, pyrite, rutile, uvite, and graphite, in the mining area (Grew, 1994). Its formation is related to the tertiary collision between the Eurasia plate and the Indian Subcontinent in the Himalayan Orogenic Belt (Garnier et al., 2006; Malsy and Klemm, 2010).

While there has been no systematic and specialized spectroscopic research on samples from Kuh-i-Lal, spinel has been investigated for decades. Wood and Imbusch (1968) calculated the crystal field parameters of Cr^{3+} in spinel. Stręk et al. (1988) analyzed the ultraviolet/visible (UV-Vis) spectra and photoluminescence (PL) spectra, concluding that $MgAl_2O_4$ spinel was affected by the spin-allowed transitions $^4A_{2g} \rightarrow {}^4T_{2g}$ and $^4A_{2g} \rightarrow {}^4T_{1g}$ of Cr^{3+} ions. Dickson and Smith (1976) analyzed the combination of UV-Vis and Mössbauer spectra of spinel at room temperature, explaining the effect of iron on the optical spectra. Hålenius et al. (2010) used the Racah B parameter, which can be calculated from the energies of bands on UV-Vis spectra, to prove that the number of Cr-O bonds was related to Cr^{3+} content. Taran et al. (2005) and Fregola et al. (2014) studied the spectra of Fe^{2+} and Fe^{3+} in gahnite-hercynite and found that the *d-d* absorption spectra of Fe^{2+} in the near-infrared region are related to pressure. Andreozzi et al. (2019) classified two categories of color: (1) iron-poor orange, red, and magenta spinel and (2) iron-rich pink, blue, and green spinel. The former group of colors is mainly caused by the spin-allowed transition of Cr^{3+} and V^{3+} ions, while the latter group is due to the function of Fe_{tot} and Fe^{3+}.

A topic of particular importance to the gem and jewelry trade is the heat treatment of spinel to improve its appearance. We already have some knowledge about the heating process used: Mohler and White (1995) studied the PL spectrum of Cr^{3+} of spinel and found that the change of temperature invariably affects the phonon line structure of Cr^{3+}. Neutron diffraction, Raman spectroscopy, single-crystal diffraction, and other methods were used to explore the change of cation distribution and lattice parameters of spinel during the heating process (Peterson et al., 1991; Cynn et al., 1992; Redfern et al., 1999; Méducin et al., 2004; Minh and Yang, 2004; Uchida et al., 2005; Slotznick and Shim, 2008). Widmer et al. (2015) analyzed the changes in the PL spectrum and Raman spectrum of red spinel under heating conditions. It was found that the lattice parameters changed with temperature and pressure, resulting in a sudden change of intensity and full width at half maxima (FWHM) of peaks in the PL spectrum.

Spinel is a traditionally popular gem featuring high transparency and desirable colors. Since 2000, it has seen a large price increase in China. The mines of Kuh-i-Lal have been an important source for centuries (the famous Black Prince's ruby from the British Imperial State Crown is said to have been mined there). To date, however, there has been no systematic study on the characteristic spectroscopy of spinel from this mining area. In this paper, the spectroscopic thermal variations and chromophoric mechanism of pink spinel reportedly from Kuh-i-Lal were studied using UV-Vis spectroscopy, PL spectroscopy, and mid-infrared spectroscopy, combined with laser ablation–inductively coupled plasma–mass spectroscopy (LA-ICP-MS) and heat treatment, to reveal the structural changes following different heat treatment temperatures and the function of internal chromophoric elements.

Figure 1. This faceted spinel was mined in the Kuh-i-Lal deposit of Tajikistan and weighs slightly more than 20 ct. Photo by Vincent Pardieu/Gübelin Gem Lab (2008); courtesy of Edigem.

MATERIALS AND METHODS

In this study, we collected 20 gem-quality pink spinel samples reportedly from the Kuh-i-Lal region. The samples were purchased by author DS during field trips to the Namak Mandi gem market in Peshawar (Pakistan) in 2000 and 2001 and from Tajik, Afghan, and Pakistani dealers in Bangkok between 2014 and 2019. Samples ranged from 0.781 to 4.360 ct. Refractive index measurements were acquired with a desktop refractometer on all samples, and hydrostatic specific gravity values were obtained on the same samples. Each crystal had either one or two polished windows, ensuring that internal characteristics could be clearly observed and spectral testing could be carried out. The sample details are listed in table 1.

TABLE 1. Description and gemological characteristics of pink spinel from Kuh-i-Lal, Tajikistan.

Sample no.	Photo	Color	Weight (ct)	Refractive index	Specific gravity
SP-01		Deep pink	1.866	1.714	3.56
SP-02		Pink	1.265	1.713	3.55
SP-03		Light pink	1.260	1.712	3.57
SP-04		Pink	1.178	1.714	3.57
SP-05		Deep pink	1.900	1.711	3.58
SP-06		Pink	0.971	1.710	3.57
SP-07		Light pink	0.781	1.712	3.57
SP-08		Pink	1.995	1.712	3.56
SP-09		Deep pink	1.909	1.713	3.57
SP-10		Pink	0.849	1.713	3.55

Spectroscopy was performed at the Laboratory of Gem and Technological Materials, Tongji University in Shanghai. PL spectra were obtained between 560 and 850 nm using a confocal Raman spectrometer (Horiba Jobin Yvon LabRAM HR Evolution). All spectra were measured using an excitation wavelength of 532 nm. The acquisition time was 5 s, and two scans with the 50× objective of the microscope were performed. All spectra were collected using a power of 50 mW and a confocal aperture of 50 µm.

Twenty samples for UV-Vis absorbance spectra were cut and polished on two parallel sides. Each sam-

TABLE 1 (continued). Description and gemological characteristics of pink spinel from Kuh-i-Lal, Tajikistan.

Sample no.	Photo	Color	Weight (ct)	Refractive index	Specific gravity
SP-13		Pink	2.101	1.713	3.57
SP-29		Deep pink	3.345	1.713	3.56
SP-30		Light pink	2.220	1.711	3.55
SP-34		Pink	4.360	1.712	3.57
SP-36		Deep pink	2.870	1.710	3.55
SP-37		Light pink	0.823	1.710	3.58
SP-42		Light pink	1.930	1.712	3.55
SP-43		Light pink	1.218	1.711	3.58
SP-47		Deep pink	1.141	1.711	3.58
SP-50		Deep pink	2.760	1.713	3.55

ple had a thickness of 1.52 to 2.54 mm. UV-Vis absorption spectra were obtained with a UV-Vis spectrometer (PerkinElmer Lambda 650s). The spectra were obtained with a resolution of 1 nm, a scan speed of 266.75 nm/min, a photomultiplier (PMT) response of 0.4 s, and a scan range of 300–800 nm.

Mid-infrared reflectance spectra were measured with a Bruker Tensor 27 FTIR spectrometer equipped with a reflectance accessory. The spectra were recorded with a resolution of 4 cm^{-1} and 32 scans. The scan speed was 10 kHz with a raster of 6 mm in the range of 400–4000 cm^{-1}. The absorbance of the

TABLE 2. Transition metal element contents of pink spinel from Kuh-i-Lal, obtained by LA-ICP-MS (the range of values for each sample is based upon three spots).

Sample	MgO (wt.%)	Al_2O_3 (wt.%)	V (ppmw)	Cr (ppmw)	Mn (ppmw)	Fe (ppmw)	Co (ppmw)
SP-01	29.9–30.1	68.9–69.0	201–205	753–894	108.4–116.2	3577.8–3577.8	1.0–1.5
SP-02	29.6–29.9	69.1–69.4	317–355	426–444	123.9–123.9	2411.1–2488.9	0.7–9.6
SP-03	29.8–30.1	68.8–69.3	331–347	242–272	123.9–131.7	2411.1–2488.9	0.6–1.0
SP-04	30.2–30.3	68.7–68.9	354–391	457–501	108.4–123.9	2411.1–2722.2	0.6–1.2
SP-05	29.9–30.1	68.9–69.2	286–300	432–699	123.9–123.9	2411.1–2566.7	0.5–0.9
SP-06	30.2–30.3	68.5–68.8	314–347	469–873	123.9–131.7	2333.3–2644.4	0.7–1.4
SP-07	29.9–30.1	68.9–69.3	232–314	384–766	123.9–123.9	2255.6–2488.9	0.6–1.2
SP-08	30.3–30.5	68.7–68.8	286–311	290–338	123.9–131.7	2100.0–2488.9	0.8–1.1
SP-09	29.8–29.9	69.1–69.1	187–192	630–699	108.4–108.4	3577.8–3733.3	0.8–1.5
SP-10	29.1–30.1	69.0–69.9	268–283	371–412	108.4–116.2	2644.4–2722.2	0.3–0.5
SP-13	30.1–30.4	69.0–69.3	283–288	182–365	116.2–116.2	2488.9–2644.4	0.6–0.9
SP-29	29.8–30.1	68.9–69.2	271–273	669–695	108.4–108.4	2722.2–3188.9	0.7–0.8
SP-30	30.3–30.7	68.6–68.8	293–446	253–421	108.4–116.2	1944.4–2333.3	0.8–1.2
SP-34	30.4–30.5	68.4–68.6	318–332	368–446	123.9–131.7	2644.4–2877.8	0.3–0.8
SP-36	29.5–29.8	69.2–69.6	378–394	397–551	116.2–116.2	2566.7–2722.2	0.7–0.8
SP-37	30.7–31.0	68.2–68.5	358–373	136–178	100.7–108.4	1633.3–2177.8	0.3–1.0
SP-42	30.5–30.7	68.4–68.4	254–340	365–426	123.9–123.9	2722.2–2800.0	0.6–1.3
SP-43	29.6–30.4	68.6–69.6	265–339	318–464	108.4–116.2	2100.0–2566.7	0.6–0.9
SP-47	30.0–30.5	68.4–68.9	153–165	701–920	100.7–108.4	3655.6–3655.6	0.8–1.0
SP-50	29.8–30.1	69.0–69.3	262–269	303–364	116.2–116.2	2488.9–2722.2	0.5–1.0
Detection limits	0.0015	0.0032	0.5	52.9	5.4	124.4	0.7
Pink samples (Andreozzi et al., 2019)	—	—	68–815	68–1436	154.9–542.1	2722.2–27377.8	—
Magenta samples (Andreozzi et al., 2019)	—	—	476–952	1505–7115	0–154.9	1011.1–4900.0	—

Note: ppmw = parts per million by weight.

samples was calculated from the reflectance data through Kramers-Kronig analysis.

Trace element analyses were performed on all 20 samples using LA-ICP-MS at Wuhan Sample Solution Analytical Technology Co., China, using an Agilent 7900 mass spectrometer with a GeoLas HD coherent excimer laser ablation system (193 nm ablation wavelength and 5 Hz frequency with an energy of 80 mJ).

Three measuring points (64 µm diameter) were selected for each sample. The data were calibrated using multiple external standards: NIST SRM 610, NIST SRM 612, BCR-2G, BHVO-2G, and BIR-2G. The ICPMSDataCal 10.8 software was used for data processing. Detailed information on the instrument setting and data processing follows the description of Liu et al. (2008).

Because spinel contains many crevices, it is easy for samples to fracture during the heating process. Two samples with sufficient clarity (SP-05 and SP-34) were selected for heat treatment, one of which (SP-34) was cut into four small pieces of about 2 × 2 × 1 mm. These five pieces of crystal (SP-05, SP-34.1, SP-34.2, SP-34.3, and SP-34.4) were heated to temperatures of 300°, 500°, 600°, 650°, 700°, 750°, 775°, 800°, 825°, 850°, 875°, 900°, and 1000°C at a heating rate of 10°C/min. After reaching the target temperature, the samples were annealed for one hour, and then the pieces were cooled to room temperature at a rate of 20°C/min in the switched-off furnace. Unfortunately, sample SP-34.4 broke apart during the heating process, so data will only be reported for the remaining four samples. The PL and mid-infrared spectra were recorded after heating to different temperatures, and the spectral measurement parameters were the same as those for samples with no heating.

The peak fitting process was evaluated using PeakFit version 4.12 (Systat Software Inc., Palo Alto, California), with the shape and width of the peaks varied. According to Taran et al. (2005), we assume that band shapes are Gaussian, and a combination of Gaussian and Lorentzian curves was used to fit these spectra. The peak analysis (FWHM and integration of R-line and N-lines) in PL spectra were calibrated using OriginPro 2018 (OriginLab, Northampton, Massachusetts).

RESULTS

Chemical Composition. Spinel with the ideal structure $MgAl_2O_4$ is allochromatic, and therefore pure spinel is colorless. Color is caused by transition metal elements in the crystal lattice. One detailed study (Andreozzi et al., 2019) divided spinel of different colors into two groups:

1. Iron-poor orange, red, and magenta spinel: colored by the combined effect of iron, chromium, and vanadium
2. Iron-rich pink, blue, and green spinel: attributed to the increase of Fe_{tot} and Fe^{3+} (Andreozzi et al., 2019).

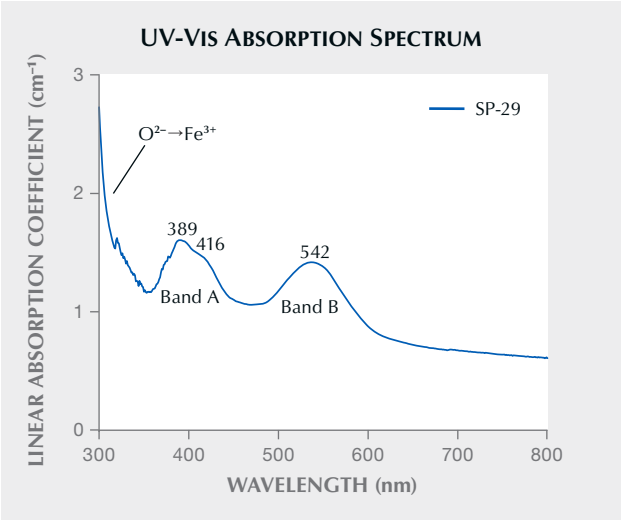

Figure 2. A typical UV-Vis absorption spectrum of pink spinel from Kuh-i-Lal.

In the present study, the main transition metal element of Kuh-i-Lal pink spinel was iron, ranging from 1633.3 to 3733.3 ppm. The samples also contained small amounts of chromium and vanadium. Chromium varied from 136.0 to 920.0 ppmw, and vanadium content ranged from 153.0 to 446.0 ppmw. In addition, there were other transition metal elements such as manganese (100.7–131.7 ppmw) and cobalt (0.3–9.6 ppmw). The LA-ICP-MS test results of all samples are presented in table 2.

UV-Vis Absorbance Spectra. A representative UV-Vis absorbance spectrum of pink spinel from Kuh-i-Lal is shown in figure 2. In general, the UV-Vis absorbance spectrum of spinel from this locality can be divided into three zones:

1. an absorption band at 389 nm, with a shoulder at 416 nm (band A)
2. a wide absorption band with absorption maxima at 542 nm (band B)
3. a set of weak and narrow absorption bands at around 700 nm with absorbance fluctuations

The detailed characteristics of the absorption peak at 685 nm in the third zone could not be observed with the UV-Vis spectrometer, so the peak was recorded by the photoluminescence spectrometer and described in detail below.

The deuterium lamp's emission at 319.2 nm causes the noise at 319 nm, while the noise from 319 to 370 nm is caused by the signal instability of the deuterium lamp. (The light source for the rest of the range was a tungsten lamp.)

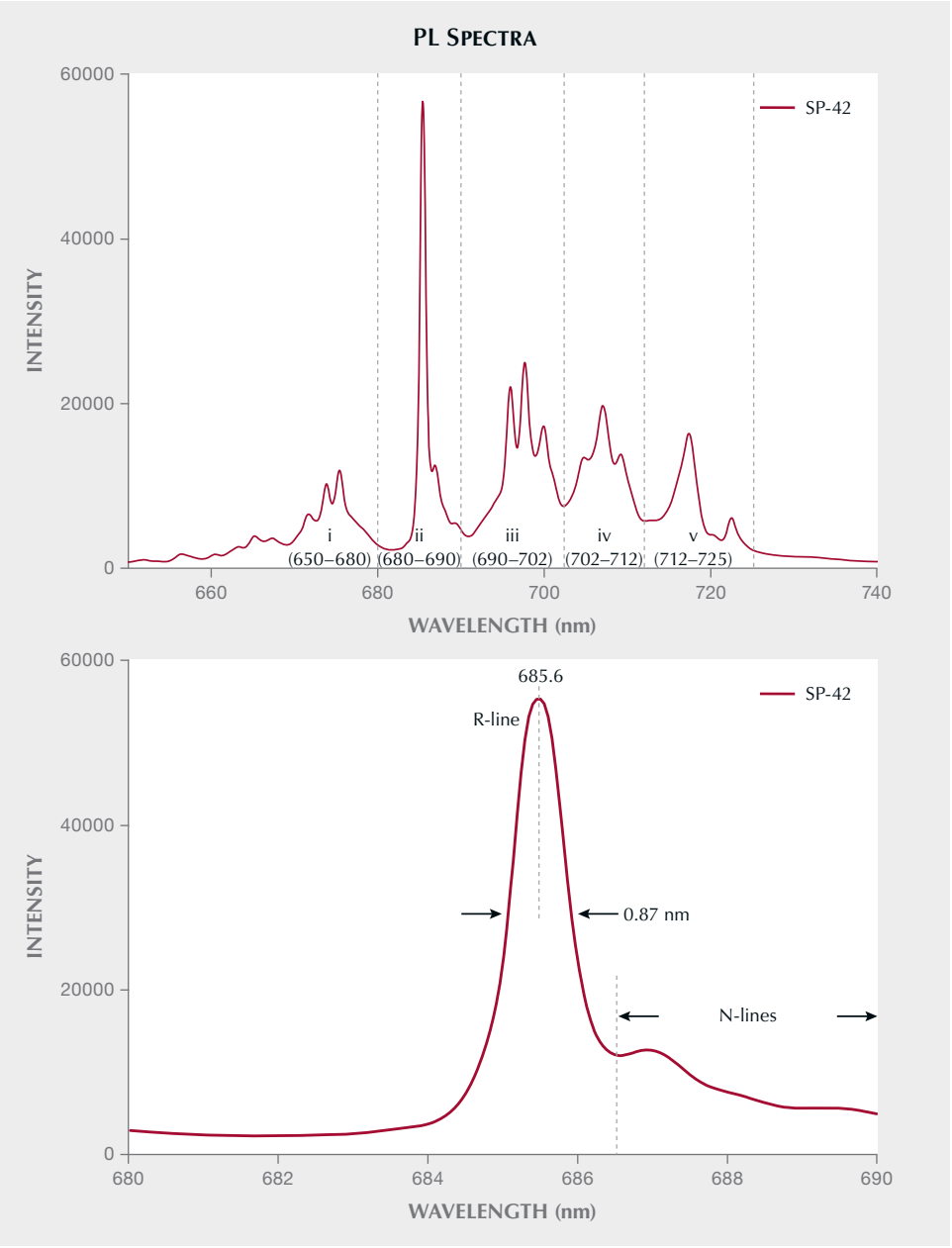

Figure 3. Top: A representative photoluminescence spectrum of Kuh-i-Lal pink spinel SP-42 at room temperature. Bottom: In region ii, the FWHM of the R-line is 0.87 nm.

The iron-poor orange, red, and magenta spinel examined by Andreozzi et al. (2019) have absorption patterns similar to those from the present study. Meanwhile, the iron-rich pink, blue, and green spinel from that earlier study have an obvious absorption band at around 458±18 nm.

PL Spectra. A typical photoluminescence spectrum of Kuh-i-Lal spinel is shown in figure 3. The PL spectra of all the samples displayed the same pattern of emission lines but with different intensities. The PL spectra of spinel from Kuh-i-Lal and Myanmar are very similar and can be divided into five regions (Malíčková et al., 2021):

i. a group of emission lines in the area of 650–680 nm (with the strongest intensities at 672, 674, and 675 nm)
ii. 680–690 nm (with the sharpest and highest emission line at 685.6 nm)
iii. 690–702 nm (including a group of emission lines of 695, 698, and 700 nm, with the strongest intensity at 698 nm)
iv. 702–712 nm (including a group of emission

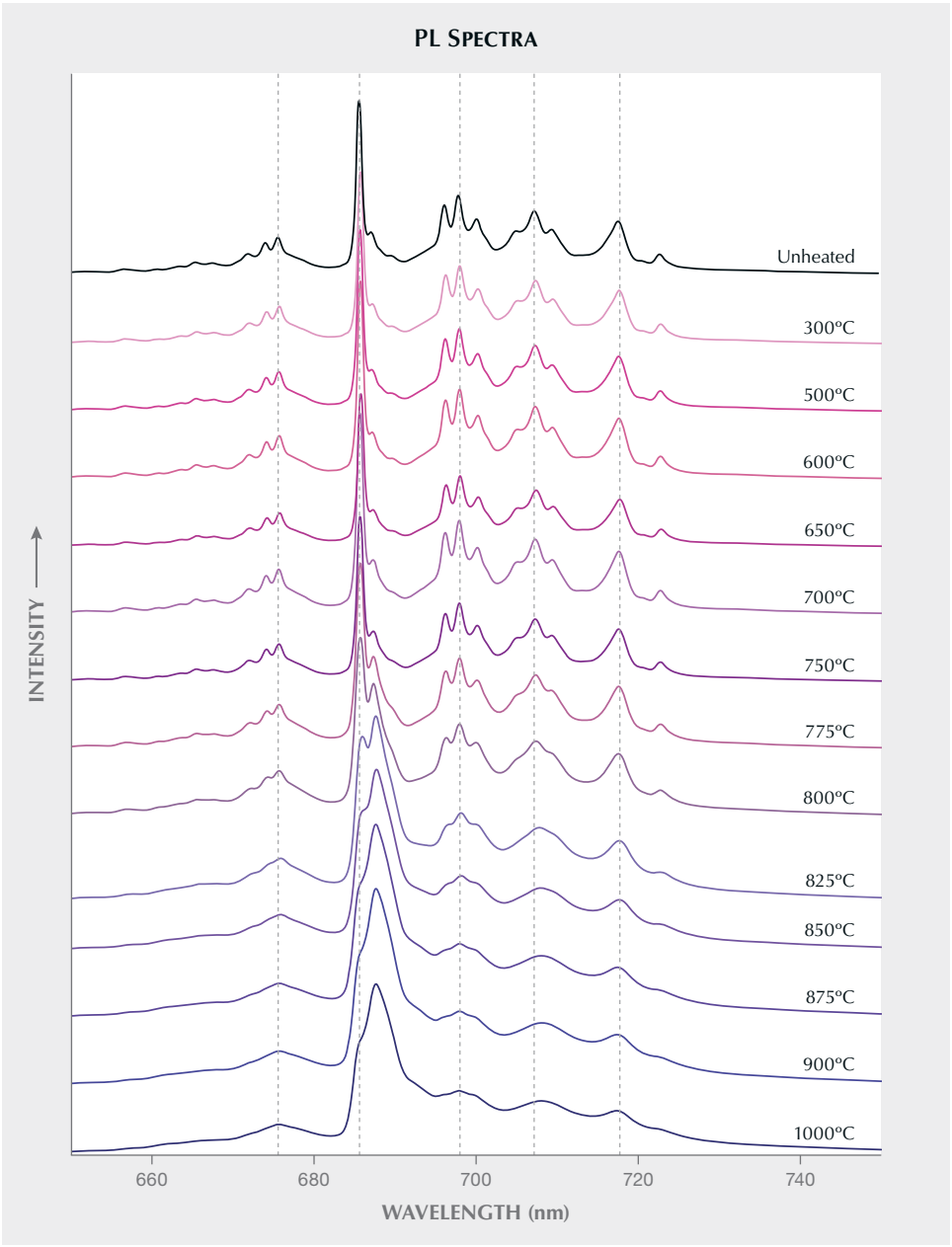

Figure 4. Photoluminescence spectra of pink spinel sample SP-05 after heating at the specified temperatures. The dashed lines represent the maxima for each peak from the different PL regions. N_1 exceeds the emission line at 685.6 nm (R-line) after heating to about 825°C, while the FWHM of these emission lines gradually widened following heating at higher temperatures.

lines of 705, 707, and 709 nm, with maxima at 707 nm)

v. 712–725 nm (including two emission lines at 717 and 722 nm)

In the PL spectra of Cr^{3+}-bearing spinel at room temperature, the R-line, a very strong and sharp emission line located at 685.6 nm (figure 3, top), is formed by the spin-forbidden transition $^2E(^2G) \rightarrow {}^4A_2(^4F)$ of Cr^{3+} (Phan et al., 2004; Widmer et al., 2015). The strength of the R-line is related to the different classes of substitutional Cr^{3+} ions, and its generation reflects the existence of ideal coordinated Cr^{3+} (Phan et al., 2004; Widmer et al., 2015), which is recorded as Cr {ideal}. Saeseaw et al. (2009) first investigated the effect of heat treatment on PL spectra of pink spinel. According to that study, the FWHM is an important parameter to identify unheated spinel, which ranges from 0.82 to 1.12 nm. The FWHM of samples in this research ranges from 0.85 to 0.93 nm. In addition to the R-line, there are also N-lines in region ii (figure 3, bottom).

The effects of heat treatment on the PL spectra of spinel sample SP-05 (figure 4) are shown in the following two respects:

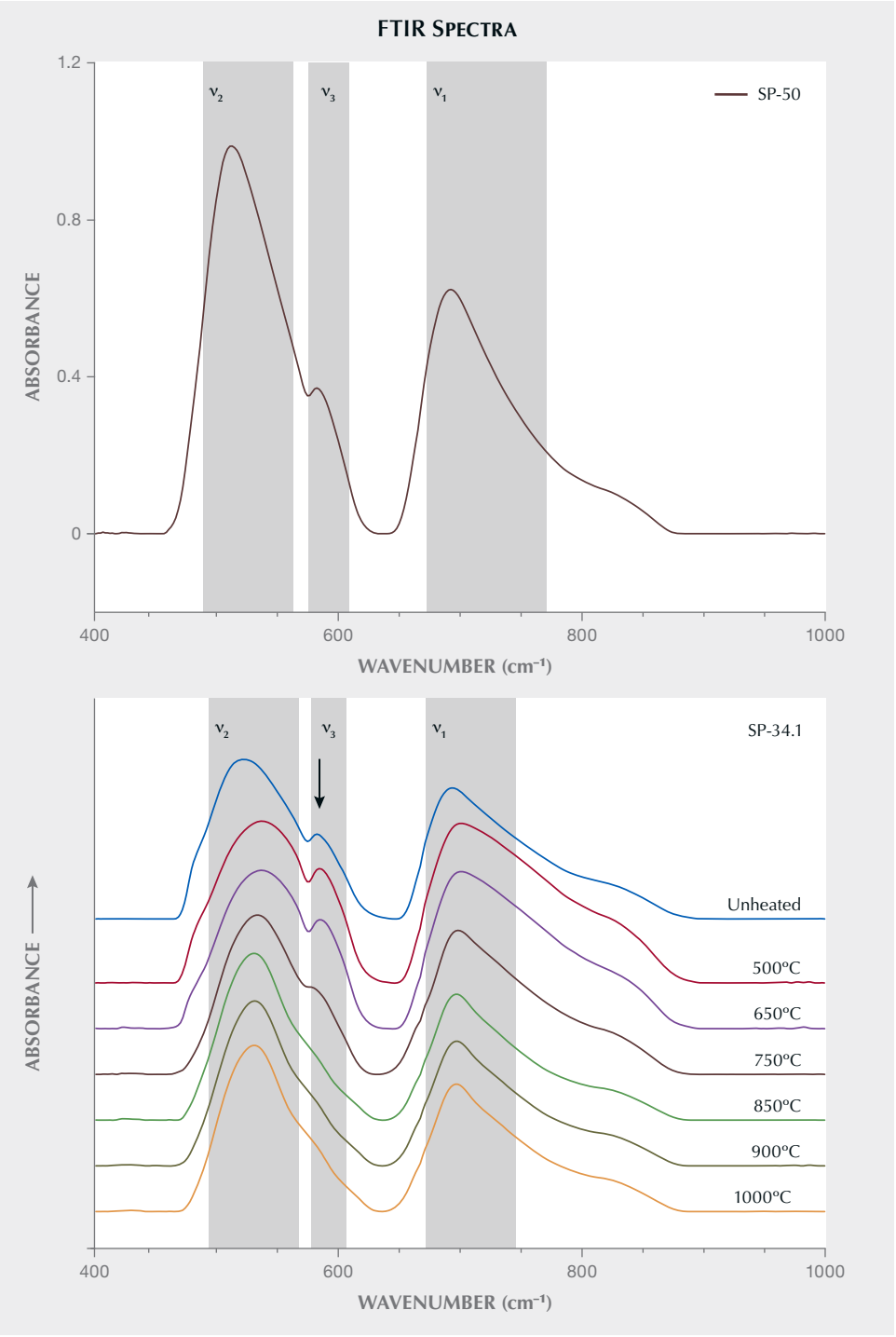

Figure 5. Top: A representative absorption spectrum (converted reflectance data) of Kuh-i-Lal unheated pink spinel. Bottom: The thermal variation of the infrared spectra (SP-34.1) following heating at the indicated temperatures. Spectra are offset vertically for clarity.

1. After heating to 750°C, the luminescence intensity at 687 nm (N_1) in region (ii) gradually increased. N_1 exceeds the emission line at 685.6 nm (R-line) after heating to about 825°C and prevails after heating up to 1000°C. The FWHM indicate a significant increase with heating. This change is no longer obvious after 850°C.
2. The baseline in parts (i), (iii), (iv), and (v) strengthened slightly following increasing heating temperature, and the FWHM of the original emission lines gradually widened simultaneously. After heating to 850°C, the spectra only display emission lines with the highest intensity at 675, 696, 698, 700, 708, and 717

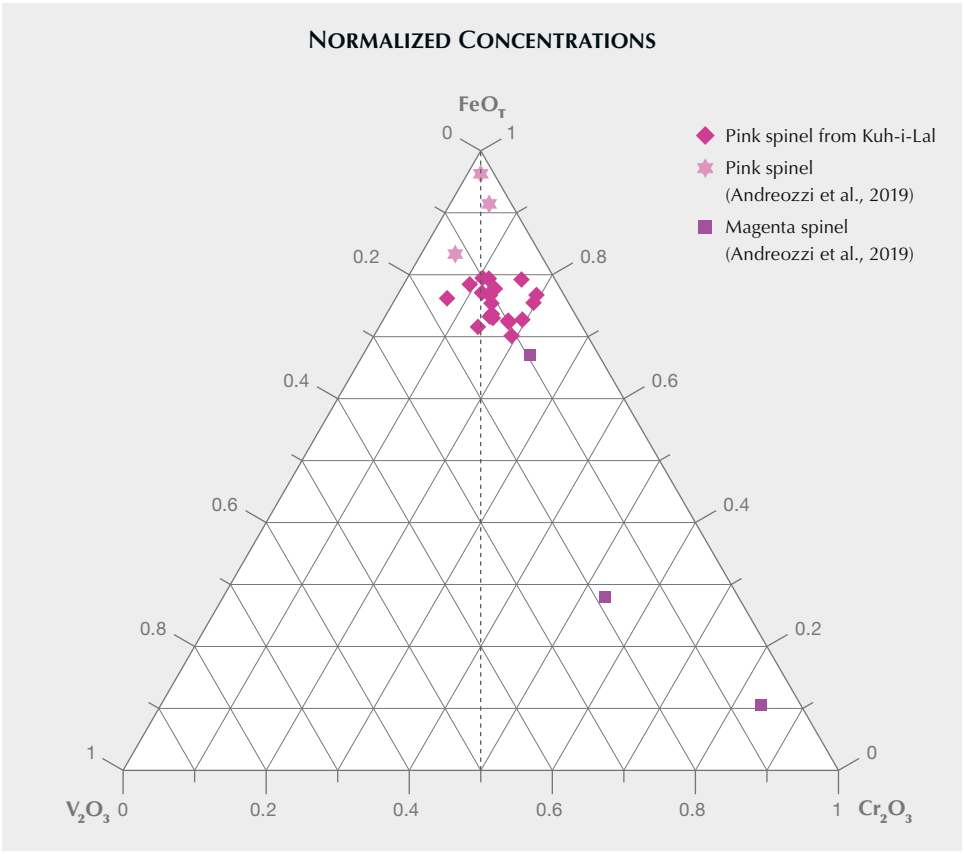

Figure 6. Normalized concentrations of FeO_T (total content of iron oxide), V_2O_3, and Cr_2O_3 for Kuh-i-Lal spinel samples (modified from Andreozzi et al., 2019). Hexagrams and squares represent samples from Andreozzi et al. (2019), while the diamonds represent pink spinel from the present study.

nm, while other lines are not distinguishable. Following heating at 1000°C, only wide emission bands at 675, 698, 708, and 717 nm are still observable.

Mid-Infrared Spectroscopy. This study only discusses the mid-infrared spectra of Kuh-i-Lal spinel in the range of 400–1000 cm^{-1}, because there is no absorption after 1000 cm^{-1}. A typical mid-infrared spectrum is shown in figure 5 (top). With no heating, there are two characteristic bands, centered near 686 cm^{-1} (ν_1) and 513 cm^{-1} (ν_2). Additionally, a shoulder can be observed at 581 cm^{-1} (ν_3). After heating to 650°C, this shoulder becomes less intense with rising temperature, and it disappears completely at 850°C (figure 5, bottom).

DISCUSSION

Coloration Mechanism. The color of spinel is assigned by the chromophoric elements in its lattice. The LA-ICP-MS results show that pink spinel from Kuh-i-Lal contains a variety of trace transition metal elements, but not all transition metal elements contribute to color. Iron-rich pink, blue, and green spinel are mainly influenced by iron, while orange, red, and magenta (including iron-poor pink) spinel are colored by the combined effect of iron, chromium, and vanadium (Andreozzi et al., 2019). In Andreozzi's electron probe microanalysis (EPMA) results, the iron content of pink and magenta spinel are similar (see table 2), but the contents of chromium and vanadium in their sample sets vary greatly because of limited samples (three samples in light pink, purplish pink, and reddish pink respectively). Compared with their samples, our samples have a lower concentration of chromium and vanadium.

As shown in figure 6, the ternary diagram reflects that the distributions of iron, chromium, and vanadium in our samples are close to those from Andreozzi for both the pink samples and one of the magenta samples. Based solely on chemical composition, it is hard to declare that the color mechanism of pink spinel in Kuh-i-Lal is caused by one of the categories mentioned by Andreozzi et al. (2019).

The UV-Vis absorption spectra reveal the chromophoric mechanism of chromium and vanadium, and the UV spectral patterns of all samples were nearly the same (see figure 2 for an example spectrum). According to Taran et al. (2014), the absorption bands of ~18,500 cm^{-1} (540.54 nm) and ~25,400 cm^{-1} (393.70

nm) can be attributed to Cr^{3+} spin-allowed transition $^4A_{2g} \rightarrow {}^4T_{2g}$ and $^4A_{2g} \rightarrow {}^4T_{1g}$. However, the absorption bands of V^{3+} also exist in this region, very close to the absorption bands of Cr^{3+}. The two strong absorption bands of V^{3+} at ~18,500 cm^{-1} and ~25,400 cm^{-1} are assigned to the *d-d* spin-allowed transitions $^3T_1(F) \rightarrow {}^3T_1(P)$ and $^3T_1(F) \rightarrow {}^3T_2(F)$, respectively (Andreozzi et al., 2019).

Following a peak-fitting procedure outlined by Andreozzi et al. (2019) in order to separate (deconvolute) the overlapping absorption bands, six fitted peaks were distinguished using PeakFit 4.12, as shown in figure 7 (sample SP-42). Three absorption peaks at around 389 nm (1), 418 nm (2), and 456 nm (3) were obtained by deconvoluting the band A. Peaks (1) and (2) can be attributed to the *d-d* spin-allowed transition $^4A_{2g} \rightarrow {}^4T_{1g}(^4F)$ of Cr^{3+}, and peak (3) is caused by spin-forbidden transition $^6A_1 \rightarrow {}^4A_1$, ^4E of Fe^{3+} ions. Two other absorption peaks are obtained by fitting band B, located near 527 nm (4) and 567 nm (5), respectively. Peak (4) was assigned to $^4A_{2g} \rightarrow {}^4T_{2g}(^4F)$ of Cr^{3+}, while peak (5) was caused by the spin-allowed transition $^3T_1(^3F) \rightarrow {}^3T_2(^3F)$ of V^{3+} (Hålenius et al., 2010; Malsy and Klemm, 2010; Taran et al., 2014; Andreozzi et al., 2019). The last peak is at 674 nm (6), which can be attributed to Fe^{2+}-Fe^{3+} intervalence charge transfer, possibly strengthened by exchange-coupled pair (ECP) interactions in Fe^{3+}-Fe^{3+} clusters (Andreozzi et al., 2001). The UV-edge absorption near 300 nm is attributed to the charge transfer transition of $O^{2-} \rightarrow Fe^{3+}$ (Malsy and Klemm, 2010; Taran et al., 2014; Andreozzi et al., 2019).

Therefore, the color of pink spinel from Kuh-i-Lal is caused not only by Cr^{3+} and V^{3+}, but also by Fe^{3+} and Fe^{2+}-Fe^{3+} intervalence charge transfer.

Spectroscopic Thermal Variation Characteristics. The PL spectra of spinel mainly reflect the environment of Cr^{3+} ions (Widmer et al., 2015). The PL spectrum of Kuh-i-Lal pink spinel consists of an R-line, N-lines, and their phonon sidebands (PSB). The R-line located at 685.6 nm is formed by the spin forbidden transition $^2E(^2G) \rightarrow {}^4A_2(^4F)$ of ideal coordinated Cr^{3+}. It shows a very sharp emission line at room temperature (Phan et al., 2004; Widmer et al., 2015). Cr^{3+} generates a spectrum in each different class (i.e., position in the spinel lattice), including its own zero phonon line and its associated phonon sidebands. Cr^{3+} in the ideal class will also produce a phonon

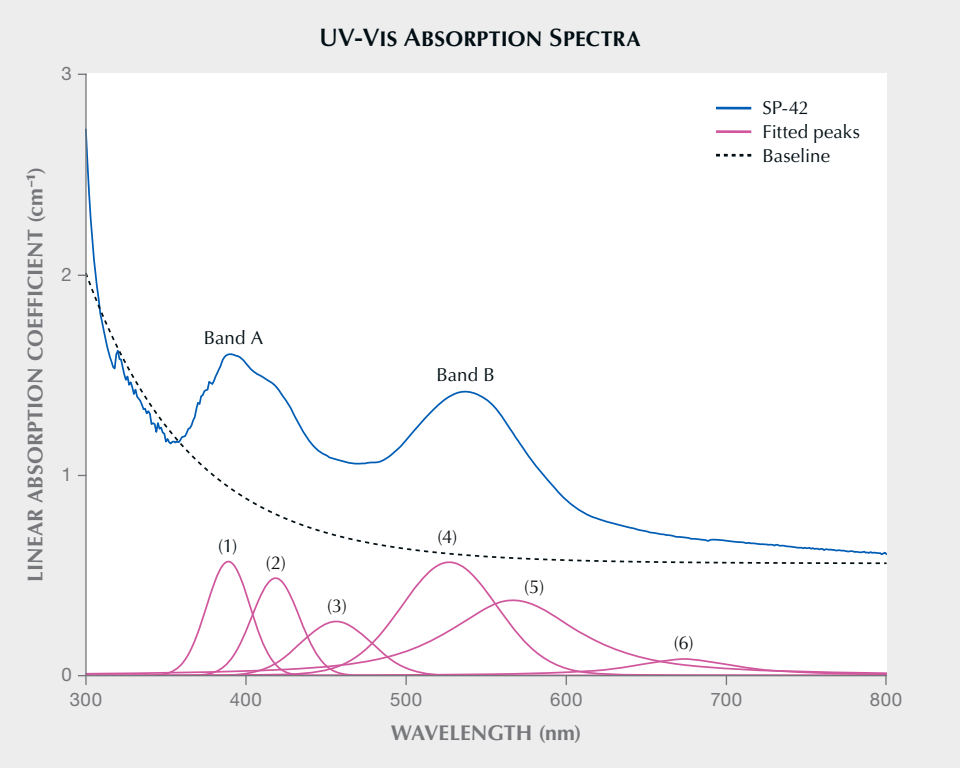

Figure 7. Curve-fitting spectra of two bands in the UV-Vis absorption spectra of sample SP-42. Results of deconvolution (pink lines) of the two bands in the absorption spectrum (blue line) of sample SP-42. The dashed line is the baseline for curve-fitting. The goodness of fit (GOF) is 0.97.

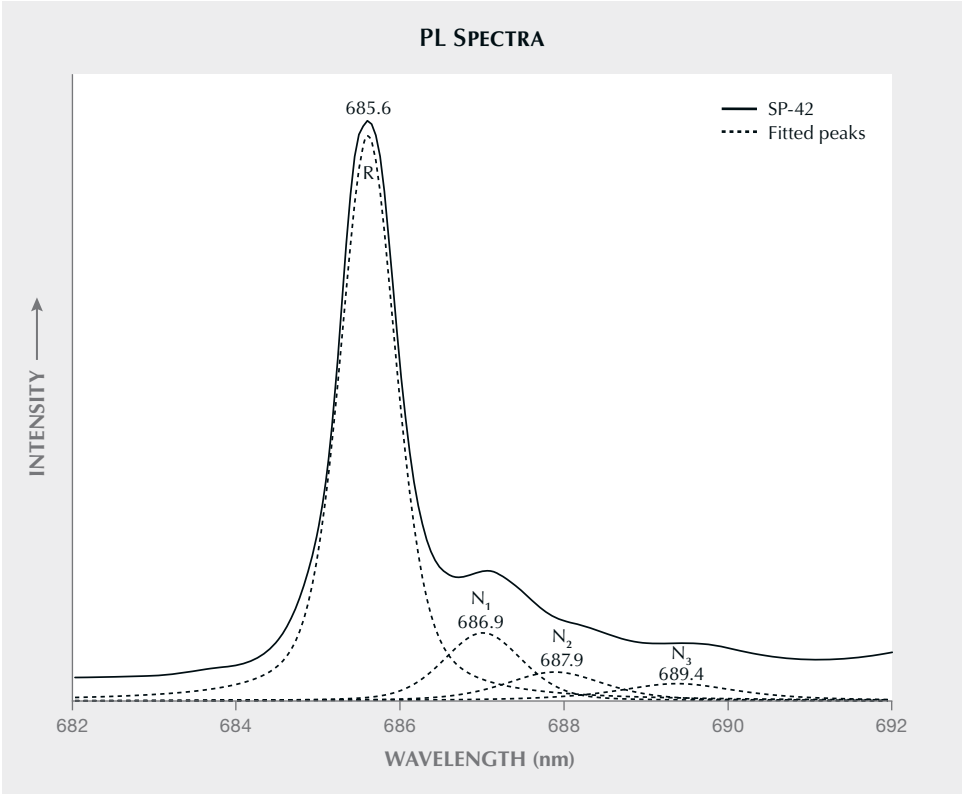

Figure 8. Curve-fitting results of PL spectra (collected at room temperature). The solid line is the PL spectrum of SP-42, and the dashed lines are the deconvoluted peaks of this unheated sample.

sideband known as R-PSB, which are phonon sidebands of the R-line. However, the anti-Stokes line of R-PSB cannot be observed at room temperature (Mikenda and Preisinger, 1981a). Lines that are neither R-line nor R-PSB are called N-lines. Due to the high intensity of the R-line at room temperature, N-lines are not as obvious. According to Widmer et al. (2015), the curve-fitting results of our samples show that three N-lines—N_1 (686.9 nm), N_2 (687.9 nm), and N_3 (689.4 nm)—can be identified in the PL spectrum in the range of 680–692 nm at room temperature, as shown in figure 8. The result of our samples matched those from Widmer et al. (2015).

The tetrahedral position of standard spinel is usually occupied by divalent cations, and the octahedral position is usually occupied by trivalent cations. For the ideal CrO_6 octahedron in spinel, six B^{3+} ions occupy the octahedral cation positions of the adjacent octahedra and six A^{2+} ions occupy the tetrahedral cation positions of the adjacent tetrahedra. The Cr^{3+} in ideal CrO_6 octahedron can also be written as Cr {ideal}. The PL spectrum of Cr {ideal} contains the R-line (685.6 nm) and R-PSB (phonon sideband) lines only. However, the substitutional Cr^{3+} ions can occupy the A and B positions at the same time in unheated spinel. The cation distribution of the substitutional Cr^{3+} ions results in a number of different Cr^{3+} classes. There are 48 classes besides Cr {ideal}, and the distortion of [CrO_6] is described by the degree of inversion (*i*), which is the ratio of A^{2+} in tetrahedral positions and A^{2+} in both tetrahedral and octahedral positions. Mikenda and Preisinger (1981b,c) established the curve of the degree of inversion (*i*) and different Cr^{3+} classes. The degree of inversion of unheated spinel is usually below 0.1. Within this threshold, the greater the *i* value, the lower the proportion of Cr {ideal}, the higher the degree of lattice disorder, the stronger the intensity of N-lines, and the lower the R-line intensity.

There are two causes of the formation of N-lines: the content of impurity ions (type I) and the defect of the main lattice (type II). The N-lines caused by type I do not change with the lattice parameters of the host crystal but are only affected by the Cr^{3+} content in spinel. Therefore, in order to identify the attribution of N-lines, we only need to determine whether the strength of N-lines changes with chromium content.

According to the comparison between the Cr^{3+} ion content obtained by LA-ICP-MS and the integral of normalized R-line and N-lines (680–692 nm), it was found in this study that the increase of Cr^{3+} ion content in the sample has no effect on the strength of the

R-line and N-lines (figure 9). Therefore, we can exclude type I as the cause of N-lines in the PL spectrum of Kuh-i-Lal spinel. Therefore, we determined that the N-lines are caused by lattice defects. The normalized R-line integral does not change with the increase of Cr^{3+} ions, indicating that the proportion of Cr {ideal} and the degree of distortion vary little with heating.

With no heating, the PL spectrum at 680–692 nm mainly shows the R-line at 685.6 nm and the N_1 line at 686.9 nm, which gradually becomes dominant after heating (see figure 4). This is because heating disturbs the lattice of the host spinel, which leads to the original Cr {ideal} transfer to other non-ideal classes.

The FWHM is calculated based on the position of N_1 since it is dominant among the N-lines. The temperature dependence of the FWHM of sample SP-05 upon heat treatment is presented in figure 10. The FWHM of the R-line and N-lines did not change significantly at first; it increased slightly after heating at 600°C. After heating to 750°C, the FWHM of the R-line and N_1 continued to widen. After heating to 825°C, these two peaks were overlapping and difficult to separate. The total FWHM increased slightly when the sample was heated to 900° and 1000°C, and the corresponding PL spectra show a wide and overlapping band. Most of the original emission lines in figure 8 are difficult to distinguish after heating above 825°C.

High-temperature conditions significantly affect the classes of Cr^{3+} ions in spinel. Figure 11 shows the temperature dependence of the integral ratio of the R-line and N-lines (in the range of 680–692 nm). After heating to temperatures less than 600°C, the ratio of the integral areas of the R-line and N lines increased slightly. At 600°C, the ratio of integral areas of the R-line to N-lines decreased slightly, dropping significantly after heating to 750°C and decreasing slightly again after heating above 825°C. In this interval of 75°C, the ratio of integral areas of the two is almost linear. The equation between temperature and the ratio of integral areas of the two in this range can be derived:

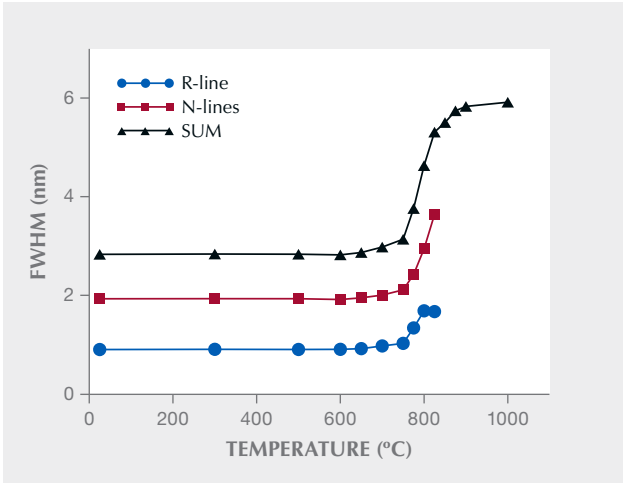

Figure 10. The trend of FWHM of the R-line and N-lines (680–692 nm) for sample SP-05 during the heating process, where SUM represents the sum of FWHM of the R-line and all N-lines.

Figure 9. After integration of the normalized R- and N-lines, the impact of chromium content is more easily observed.

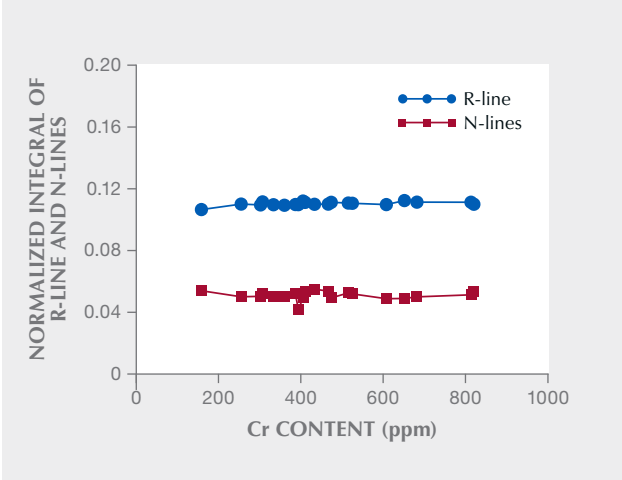

Figure 11. Temperature dependence of the ratio of integral areas of the R-line and N-lines (680–692 nm).

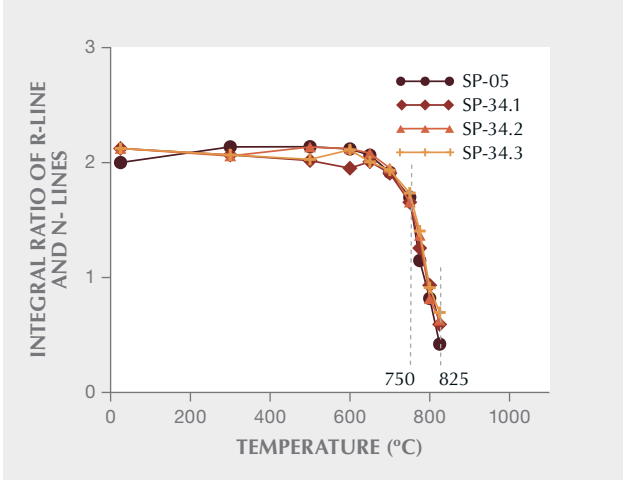

Figure 12. This pink spinel crystal in matrix from Kuh-i-Lal measures 13.82 × 12.54 mm, while the faceted gem from the same locality weighs 22.76 ct. Photo by Robert Weldon/GIA; courtesy of Pala International.

SP-05: $R = -0.01665T + 14.131$ (1) $R^2 = 0.989$
SP-34.1: $R = -0.01405T + 12.172$ (2) $R^2 = 0.998$
SP-34.2: $R = -0.01453T + 12.559$ (3) $R^2 = 0.967$
SP-34.3: $R = -0.01443T + 12.554$ (4) $R^2 = 0.981$

where R symbolizes the value of the ratio of integral areas of the R-line and N-lines, and T is the temperature. The linear change of the ratio of integral areas can explain the transition of Cr^{3+} ions from ideal to non-ideal classes in similar amounts in the temperature range of 750°– 825°C. After heating to temperatures above 825°C, the ratio of integral areas changes less dramatically than in the 750°–825°C range. At 850°C and above, the R-line and N-lines cannot be deconvoluted.

The mid-infrared spectra of spinel can be characterized by two bands at around 686 cm^{-1} (ν_1) and 513 cm^{-1} (ν_2), which are related to the bond energy between cations and oxygen in the octahedral lattice. The band at around 581 cm^{-1} (ν_3) is assigned to the complex vibration of the octahedral and tetrahedral lattices, especially the octahedral lattice vibration (Preudhomme and Tarte, 1971a,b,c, 1972).

Figure 5 (bottom) shows that ν_3 changes markedly during the heating process: The intensity of ν_3 begins to decrease with rising temperature after heating up to 650°C and almost disappears after heating to 850°C. This could provide additional evidence to distinguish between heat-treated and untreated spinel. However, the frequency of ν_1 and ν_2 fluctuate with increasing temperature, and no obvious change pattern can be observed.

Widmer et al. (2015) measured the crystal parameters of spinel before and after heat treatment using sin-

gle crystal X-ray diffraction. When heated from room temperature to 1100°C, the octahedral M-O bond length changed from 1.9226 to 1.9333 Å, and the tetrahedral T-O bond length changed from 1.9361 to 1.9130 Å. At a temperature of 650°C, the M-O and T-O bond lengths were equal at 1.927 Å (Widmer et al., 2015).

During the heating process, the difference between the two bond lengths decreases gradually. In this study, ν_3 starts to change at 650°C, which indicates that the strength and frequency of ν_3 are related to the relative length of M-O and T-O bonds. When the length of the M-O bond grows longer than that of T-O, ν_3 gradually decreases and finally disappears.

CONCLUSIONS

The main trace element of pink spinel from Kuh-i-Lal in Tajikistan (figure 12) is iron, though it also contains small amounts of chromium, vanadium, manganese, and cobalt. The chromium content is higher than that of vanadium in most samples, but in some light pink samples the chromium content is lower than that of vanadium. Pink spinel from Kuh-i-Lal owes its color to the presence of Cr^{3+}, V^{3+}, Fe^{3+}, and Fe^{2+}-Fe^{3+} intervalence charge transfer. The characteristic band A can be attributed to the spin-allowed transition $^4A_{2g} \rightarrow {}^4T_{1g}(^4F)$ in Cr^{3+} and spin-forbidden transition $^6A_1 \rightarrow {}^4A_1$, ^4E of Fe^{3+} ions, while band B in the visible region is caused by spin-allowed *d-d* transition $^4A_{2g} \rightarrow {}^4T_{2g}(^4F)$ of Cr^{3+} and $^3T_1(^3F) \rightarrow {}^3T_2(^3F)$ of V^{3+}. The edge of the spectra at 674 nm can be attributed to Fe^{2+}-Fe^{3+} intervalence charge transfer.

With no heating, the PL spectrum of Kuh-i-Lal pink spinel is a group of emission lines characterized by the R-line and N-lines produced by Cr^{3+} ions. The intensity of the R-line and N-lines is independent of the Cr^{3+} ion content. After heating to 750°–825°C, the intensity of the N_1 peak increases gradually, and the FWHM of the R-line and N-lines (in the range of 680–692 nm) increases continuously. There is a strong linear relationship between the ratio of integral areas of the R-line and N-lines (680–692 nm) and temperature in this 75° range, and Cr {ideal} changes to other non-ideal chromium classes at an almost constant rate.

Reflectance mid-infrared spectra showed that when heated to 650°C, ν_3 gradually starts to disappear before disappearing completely after heating at 850°C, which provide additional evidence for distinguishing heat-treated spinel. The disappearance of ν_3 at high temperature is probably related to the change of M-O and T-O bond lengths in the spinel lattice.

ABOUT THE AUTHORS

Ms. Liu is a postgraduate student, Dr. Qi is a professor of mineralogy and gemology, and Dr. Zhou is a professor of mineralogy and tectonics, at Tongji University in Shanghai. Dr. Schwarz is a visiting professor at Tongji Zhejiang College in Jiaxing, China.

ACKNOWLEDGMENTS

This research was supported by special funding from the Shanghai Science and Technology Commission (15DZ2283200, 18DZ2281300) and the Gem Discipline Development Fund. LA-ICP-MS tests were completed with the assistance of staff from Wuhan SampleSolution Analytical Technology Co., Ltd. We greatly thank the peer reviewers for providing suggestions and improving the manuscript.

REFERENCES

Andreozzi G.B., Hålenius U., Skogby H. (2001) Spectroscopic active $^{IV}Fe^{3+}$–$^{VI}Fe^{3+}$ clusters in spinel–magnesioferrite solid solution crystals: A potential monitor for ordering in oxide spinels. *Physics and Chemistry of Minerals*, Vol. 28, No. 7, pp. 435–444, http://dx.doi.org/10.1007/s002690100178

Andreozzi G.B., D'Ippolito V., Skogby H., Hålenius U., Bosi F. (2019) Color mechanisms in spinel: A multi-analytical investigation of natural crystals with a wide range of coloration. *Physics and Chemistry of Minerals*, Vol. 46, No. 4, pp. 343–360, http://dx.doi.org/10.1007/s00269-018-1007-5

Chauviré B., Rondeau B., Fritsch E., Ressigeac P., Devidal J.L. (2015) Blue spinel from the Luc Yen District of Vietnam. *G&G*, Vol. 51, No. 1, pp. 2–17, http://dx.doi.org/10.5741/GEMS.51.1.2

Cynn H., Sharma S.K., Cooney T.F. (1992) High-temperature Raman investigation of order-disorder behavior in the $MgAl_2O_4$ spinel. *Physical Review B*, Vol. 45, No. 1, pp. 500–502, http://dx.doi.org/10.1103/PhysRevB.45.500

De Souza S.S., Ayres F., Blak A.R. (2001) Simulation models of defects in $MgAl_2O_4$: Fe^{2+}, Fe^{3+} spinels. *Radiation of Effects and Defects in Solids*, Vol. 156, No. 1, pp. 311–316, http://dx.doi.org/10.1080/10420150108216911

Dickson B.L., Smith G. (1976) Low-temperature optical absorption and Mössbauer spectra of staurolite and spinel. *Canadian Mineralogist*, Vol. 14, pp. 206–215.

Fregola R.A., Skogby H., Bosi F., D'Ippolito V., Andreozzi G.B., Hålenius U. (2014) Optical absorption spectroscopy study of the causes for color variations in natural Fe-bearing gahnite: Insights from iron valency and site distribution data. *American Mineralogist*, Vol. 99, No. 11-12, pp. 2187–2195, http://dx.doi.org/10.2138/am-2014-4962

Garnier V., Giuliani G., Maluski H., Ohnenstetter D., Schwarz D. (2006) Ar-Ar and U-Pb ages of marble-hosted ruby deposits from Central and Southeast Asia. *Canadian Journal of Earth Science*, Vol. 43, No. 4, pp. 509–532, http://dx.doi.org/10.1139/E06-005

Giuliani G., Fallick A.E., Boyce A.J., Pardieu V., Pham V.L. (2017) Pink and red spinels in marble: Trace elements, oxygen isotopes, and sources. *Canadian Mineralogist*, Vol. 55, No. 4, pp. 743–761, http://dx.doi.org/10.3749/canmin.1700009

Hålenius U., Andreozzi G.B., Skogby H. (2010) Structural relaxation around Cr^{3+} and the red-green color change in the spinel (sensu stricto)-magnesiochromite ($MgAl_2O_4$-$MgCr_2O_4$) and gahnite-zincochromite ($ZnAl_2O_4$-$ZnCr_2O_4$) solid-solution series. *American Mineralogist*, Vol. 95, No. 4, pp. 456–462, http://dx.doi.org/10.2138/am.2010.3388

Hubbard M.S., Grew E.S., Hodges K.V., Yates M.G., Pertsev N.N. (1999) Neogene cooling and exhumation of upper-amphibolite-facies 'whiteschists' in the Southwest Pamir Mountains, Tajikistan. *Tectonophysics*, Vol. 305, No. 1-3, pp. 325–337, http://dx.doi.org/10.1016/S0040-1951(99)00012-8

Lenaz D., Lughi V. (2013) Raman study of $MgCr_2O_4$-$Fe^{2+}Cr_2O_4$ and $MgCr_2O_4$-$MgFe_2^{3+}O_4$ synthetic series: The effects of Fe^{2+} and Fe^{3+} on Raman shifts. *Physics and Chemistry of Minerals*, Vol. 40, No. 6, pp. 491–498, http://dx.doi.org/10.1007/s00269-013-0586-4

Liu Y.S., Hu Z.C., Gao S., Günther D., Xu J., Gao C.G., Chen H.H. (2008) In situ analysis of major and trace elements of anhydrous minerals by LA-ICP-MS without applying an internal standard. *Chemical Geology*, Vol. 257, No. 1-2, pp. 34–43, http://dx.doi.org/10.1016/j.chemgeo.2008.08.004

Long P.V., Giuliani G., Fallick A.E., Boyce A.J., Pardieu V. (2018) Trace elements and oxygen isotopes of gem spinels in marble from the Luc Yen - An Phu Areas, Yen Bai Province, North Vietnam. *Vietnam Journal of Earth Sciences*, Vol. 40, No. 2, pp. 165–177, http://dx.doi.org/10.15625/0866-7187/40/2/12241

Malíčková I., Bačík P., Fridrichová J., Hanus R., Illášová L., Štubna J., Furka D., Furka S., Škoda R. (2021) Optical and luminescence spectroscopy of varicolored gem spinel from Mogok, Myanmar and Lục Yên, Vietnam. *Minerals*, Vol. 11, No. 2, pp. 1–13, http://dx.doi.org/10.3390/min11020169

Malsy A., Klemm L. (2010) Distinction of gem spinels from the Himalayan Mountain Belt. *Chimia*, Vol. 64, No. 10, pp. 741–746, http://dx.doi.org/10.2533/chimia.2010.741

Malsy A.K., Karampelas S., Schwarz D., Klemm L., Armbruster T., Tuan D.A. (2012) Orangey-red to orangey-pink gem spinels from a new deposit at Lang Chap (Tan Huong-Truc Lau), Vietnam. *Journal of Gemmology*, Vol. 33, No. 1, pp. 19–27.

Méducin F., Redfern S.A.T., Godec Y.L., Stone H.J., Tucker M.G., Dove M.T., Marshall W.G. (2004) Study of cation order-disorder in $MgAl_2O_4$ spinel by in situ neutron diffraction up to 1600 K and 3.2 GPa. *American Mineralogist*, Vol. 89, No. 7, pp. 981–986, http://dx.doi.org/10.2138/am-2004-0708

Mikenda W., Preisinger A. (1981a) N-lines in the luminescence spectra of Cr^{3+}-doped spinels (I) Identification of N-lines. *Journal of Luminescence*, Vol. 26, No. 1-2, pp. 53–66, http://dx.doi.org/10.1016/0022-2313(81)90169-1

——— (1981b) N-lines in the luminescence spectra of Cr^{3+}-doped spinels (II) Origins of N-lines. *Journal of Luminescence*, Vol. 26, No. 1-2, pp. 67–83, http://dx.doi.org/10.1016/0022-2313(81)90170-8

——— (1981c) N-lines in the luminescence spectra of Cr^{3+}-doped spinels (III) Partial spectra. *Journal of Luminescence*, Vol. 26, No. 1-2, pp. 85–98, http://dx.doi.org/10.1016/0022-2313(81)90171-X

Minh N.V., Yang I.S. (2004) A Raman study of cation-disorder transition temperature of natural $MgAl_2O_4$ spinel. *Vibrational Spectroscopy*, Vol. 35, No. 1-2, pp. 93–96, http://dx.doi.org/10.1016/j.vibspec.2003.12.013

Mohler R.L., White W.B. (1995) Influence of structural order on the luminescence of oxide spinels: Cr^{3+}-activated spinels. *Journal of the Electrochemical Society*, Vol. 142, No. 11, pp. 3923–3927, http://dx.doi.org/10.1149/1.2048435

Peterson R.C., Lager G.A., Hitterman R.L. (1991) A time-of-flight neutron powder diffraction study of $MgAl_2O_4$ at temperatures up to 1273 K. *American Mineralogist*, Vol. 76, No. 9-10, pp. 1455–1458.

Phan T.L., Yu S.C., Phan M.H., Han T.P.J. (2004) Photoluminescence properties of Cr^{3+}-doped $MgAl_2O_4$ natural spinel. *Journal of Korean Physical Society*, Vol. 45, No. 1, pp. 63–66.

Preudhomme J., Tarte P. (1971a) Infrared studies of spinels-I. A critical discussion of the actual interpretations. *Spectrochimica Acta Part A: Molecular and Biomolecular Spectroscopy*, Vol. 27, No. 7, pp. 961–968, http://dx.doi.org/10.1016/0584-8539(71)80179-4

——— (1971b) Infrared studies of spinels-II. The experimental bases for solving the assignment problem. *Spectrochimica Acta Part A: Molecular and Biomolecular Spectroscopy*, Vol. 27, No. 6, pp. 845–851, http://dx.doi.org/10.1016/0584-8539(71)80163-0

——— (1971c) Infrared studies of spinels-III. The normal II-III spinels. *Spectrochimica Acta Part A: Molecular and Biomolecular Spectroscopy*, Vol. 27, No. 9, pp. 1817–1835, http://dx.doi.org/10.1016/0584-8539(71)80235-0

——— (1972) Infrared studies of spinels-IV. Normal spinels with a high-valency tetrahedral cation. *Spectrochimica Acta Part A: Molecular and Biomolecular Spectroscopy*, Vol. 28, No. 1, pp. 69–79, http://dx.doi.org/10.1016/0584-8539(72)80013-8

Redfern S.A.T., Harrison R.J., O'Neill H.S.C., Wood D.R.R. (1999) Thermodynamics and kinetics of cation ordering in $MgAl_2O_4$ spinel up to 1600°C from in situ neutron diffraction. *American Mineralogist*, Vol. 84, No. 3, pp. 299–310, http://dx.doi.org/10.2138/am-1999-0313

Saeseaw S., Wang W., Scarratt K., Emmett J.L., Douthit T.R. (2009) Distinguishing heated spinels from unheated natural spinels and from synthetic spinels: A short review of on-going research. *GIA Research News*, https://www.gia.edu/doc/distinguishing-heated-spinels-from-unheated-natural-spinels.pdf, April 2.

Shigley J.E., Stockton C.M. (1984) 'Cobalt-blue' gem spinels. *G&G*, Vol. 20, No. 1, pp. 34–41, http://dx.doi.org/10.5741/GEMS.20.1.34

Slotznick S.P., Shim S.H. (2008) In situ Raman spectroscopy measurements of $MgAl_2O_4$ spinel up to 1400°C. *American Mineralogist*, Vol. 93, No. 2-3, pp. 470–476, http://dx.doi.org/10.2138/am.2008.2687

Stręk W., Dereń P., Jezowska-Trzebiatowska B. (1988) Optical properties of Cr^{3+} in $MgAl_2O_4$ spinel. *Physica B: Physics of Condensed Matter*, Vol. 152, No. 3, pp. 379–384, http://dx.doi.org/10.1016/0921-4526(88)90006-3

Taran M.N., Koch-Müller M., Langer K. (2005) Electronic absorption spectroscopy of natural (Fe^{2+}, Fe^{3+})-bearing spinels of spinel s. s.-hercynite and gahnite-hercynite solid solutions at different temperatures and high-pressures. *Physics and Chemistry of Minerals*, Vol. 32, No. 3, pp. 175–188, http://dx.doi.org/10.1007/s00269-005-0461-z

Taran M.N., Parisi F., Lenaz D., Vishnevskyy A.A. (2014) Synthetic and natural chromium-bearing spinels: An optical spectroscopy study. *Physics and Chemistry of Minerals*, Vol. 41, No. 8, pp. 593–602, http://dx.doi.org/10.1007/s00269-014-0672-2

Uchida H., Lavina B., Downs R.T., Chesley J. (2005) Single-crystal X-ray diffraction of spinels from the San Carlos Volcanic Field, Arizona: Spinel as a geothermometer. *American Mineralogist*, Vol. 90, No. 11-12, pp. 1900–1908, http://dx.doi.org/10.2138/am.2005.1795

Widmer R., Malsy A.K., Armbruster T. (2015) Effects of heat treatment on red gemstone spinel: Single-crystal X-ray, Raman, and photoluminescence study. *Physics and Chemistry of Minerals*, Vol. 42, No. 4, pp. 251–260, http://dx.doi.org/10.1007/s00269-014-0716-7

Wood D.L., Imbusch G.F. (1968) Optical spectrum of Cr^{3+} ions in spinels. *Journal of Chemical Physics*, Vol. 48, No. 11, pp. 5255–5263, http://dx.doi.org/10.1063/1.1668202